Bulletin of Volcanology (2018) 80: 31
https://doi.org/10.1007/s00445-018-1198-0

RESEARCH ARTICLE

Changes in heat released by hydrothermal circulation monitored during an eruptive cycle at Mt. Etna (Italy)

I. S. Diliberto[1] · E. Gagliano Candela[1] · S. Morici[1] · G. Pecoraino[1] · S. Bellomo[1] · M. Bitetto[1] · M. Longo[1]

Received: 21 March 2017 / Accepted: 24 January 2018 / Published online: 2 March 2018

Abstract

The shallow vertical temperature profile has been measured in the proximity of an eruptive fissure far about 4 km north-northeast from Mt. Etna central craters. The monitoring site was a steam-heated soil lying between a group of flank fractures on the upper northeast flank of Mt. Etna (Italy), i.e., on the northeast rift. We chose this area because it was close to an eruptive fissure, that opened in 2002 and extended from about 2500 to about 1500 m a.s.l., with our aim being to determine a connection between this fracture system and the ongoing volcanic activity. Heat flux anomalies from the ground from September 2009 to September 2012 were evaluated. Changes in the hydrothermal release—which can be related to variations in volcanic activity—are discussed and compared to the published geophysical data. The heat flux ranges varied during the pre-eruptive (from about 7 to 38 $W \times m^{-2}$), syn-eruptive (from about 3 to 49 $W \times m^{-2}$), and post-eruptive phases, with the heat released being lowest at the latter phase (from about 1 to 20 $W \times m^{-2}$). Moreover, the heat flux time variation was strongly correlated with the eruption rate from the new southeast crater between January 2011 and April 2012. The migration of magma through active conduits acts as a changing heating source for steam-heated soils located above the active fractures. Our findings suggest that tracking the heat flux above active fractures constitutes a useful investigation field for low-cost thermal monitoring of volcanic activity. Time variations in their emissions could highlight the relationship between a hydrothermal circuit and the local network of fractures, possibly indicating variation in the structural weakness of a volcanic edifice. Continuous monitoring of heat flux, combined with a realistic model, would contribute to multidisciplinary investigations aimed at evaluating changes in volcano dynamics.

Keywords Volcanic activity · Ground temperature · Heat flux · Fumaroles · Continuous monitoring

Introduction

Mt Etna (Italy) is an active volcano where eruptions occur mainly from craters located at the edifice summit (e.g. Corsaro et al. 2017). However, flank eruptions sometimes occur along three main rift - zones, (south, west and northeast rifts; NE Rift in Fig. 1) due to the lateral propagation of shallow dikes from the central conduit (Neri et al. 2011, 2016; Ruch et al. 2012, 2013). The eruptive activity is characterized by a gaseous plume, strombolian and less-frequent paroxysmal explosions, and lava flows (e.g. Bombrun et al. 2016; Bonaccorso and Calvari 2013; Calvari et al. 2011). In many other volcanic areas, groundwater, diffuse gas emissions, and the fumarole fields are used to trace hydrological circuits and chemical-and-physical exchanges with solid structures (e.g. Heasler et al. 2009). The approach, based on fluid geochemistry research, includes a lot of experimental research activities, and the references are too broad and numerous to be cited individually. Paonita et al. (2016, 2012) showed examples for Etna's groundwater flow and degassing areas, based on a wide geochemical dataset, collected since the year 2000. Some examples from other sites are: Maldonado et al. (2017) and Federico et al. (2017) for Columbian volcanoes, Peiffer et al. (2015) for El Chichon (Mexico), Inguaggiato et al. 2011 for Stromboli; Byrdina et al. 2009, for Nepal; Paonita et al., (2016), Federico et al. 2010, for Vulcano; Matsushima et al. 2003 for Iwodake; and Lardy and Tabbagh, 1993, for Vanuatu. The structural weakness of Etna's volcanic edifice has already been suggested by analyses of deformation patterns, tectonic lineaments, and other

Editorial responsibility: T. Nishimura

✉ I. S. Diliberto
iole.diliberto@ingv.it

[1] Istituto Nazionale di Geofisica e Vulcanologia, Sezione di Palermo, Via Ugo La Malfa 153, 90146 Palermo, Italy

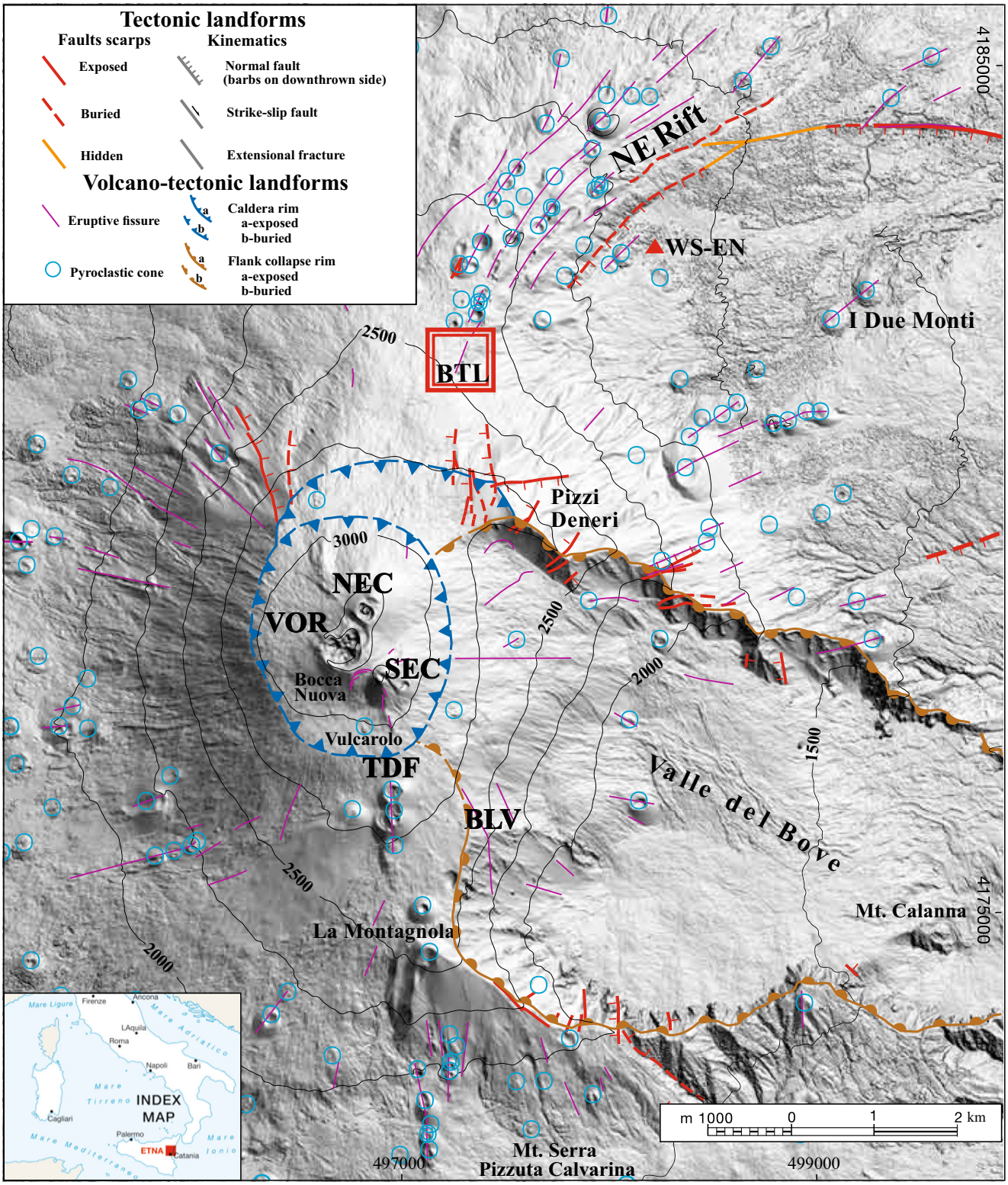

Fig. 1 Map of Mount Etna volcano showing the locations of sites mentioned in the text. The box outlined in double red indicates the monitored area. The red triangle locates the WS-EN, weather station at the Etna North. Inset bottom-left is the location of Mt. Etna in the southern Mediterranean region (modified from Azzaro et al., 2012). BTL, VOR, NEC, SEC TDF, and BLV stand, respectively, for Bottoniera Lines, Voragine, North East Crater, South East Crater, Torre del Filosofo, and Belvedere

geophysical investigations (e.g. Cannata et al. 2015; Mattia et al. 2015). Ground-based thermal monitoring can also be used to follow the real-time evolution of surface effects and to better define the geochemical fluid leakages (e.g. Mattia et al. 2015;

Revil et al. 2011; Mazot et al. 2011; Byrdina et al. 2009; Lowenstern et al. 2006; Bonaccorso et al. 2003; Patanè et al. 2003; Oskarsson et al. 1984; Sato and McGee, 1982). The hydrothermal activity on the flanks of Mt Etna changes both spatially and temporally in response to variations in magmatic pressure (e.g. Cannata et al. 2015) within the main feeding system of the volcano which, in turn, drives lava to the different eruptive vents (Paonita et al. 2012).

We here apply a method to continuously measure the shallow vertical temperature profile in a zone of steam-heated soil (SHS) on the upper northeast slope flank of Mt Etna (Italy) 4 km from the summit craters. This shows how variations in heat flux can be used to track connections between this fracture system and the ongoing volcanic activity. We set up a new monitoring site (BTL station in Figs. 2–3), and here we present the recorded variations in soil temperature and the application of the SHS monitoring method. Data (amounting to nearly 26,000 data points) were acquired hourly from September 2009 to September 2012 along a vertical soil profile (down to a depth of 60 cm) in the direction of the main component of the surface heat flow.

Geothermal anomalies at Mt. Etna: Geochemical and thermal monitoring

Etna's peripheral and summit areas have been monitored geochemically for more than 20 years (e.g., Allard et al. 1991; Bonfanti et al. 1996a,b). Large variations in geochemical signals were recorded in groundwaters during the 1991–1993 eruption (Bonfanti et al. 1996a,b). D'Alessandro et al. (1997), for example, identified a significant increase in groundwater temperatures that was related to the huge volume of magma ($> 200 \times 10^6$ m^3) erupted between 1991 and 1993 (Stevens et al. 1997; Tanguy et al. 1996; Barberi et al. 1993). Conversely, over the last two decades, no direct relationship has been found between groundwater temperatures across the lower flanks of the volcano and eruptive activity. In a geochemical investigation of the summit area, Madonia et al. (2013), however, showed a clear relationship between changes in surface thermal activity and the eruptions. Tabbagh and Trezeguet (1987) performed the earliest measurements of surface heat flux in the summit area of Mt. Etna, near Torre del Filosofo (TDF, Fig. 1). Afterwards, Aubert (1999) applied the same methodology to the same fissure system, to monitor time variations of the surface thermal release. Along the active structures, a continuous tectonic strain enhances the natural steam loss from magma and hydrothermal sources (Maucourant et al. 2014), but at the same time prevents the self-sealing phenomenon caused by mineral deposition of silica, carbonates, and/or salts that precipitate from the fluid phase (Chiodini et al. 1995; Facca and Tonani 1967). Therefore, while newly erupted products at Etna, such as lava flows and pyroclastic deposits can bury volcano-tectonic structures, the surface fluid flow can reveal structurally controlled zones beneath these superficial layers that still act as pathways for natural fluids ascending from deeper levels, variations on which can inform on the dynamics of the degassing system. As a result, Rizzo et al. (2013) were able to analyze the composition of the fluids associated with hydrothermal circulation at Etna's summit zone to obtain geochemical information about the feeding sources. Moreover, many researchers have related the time variations in diffuse CO_2 degassing from the summit and flank areas of Mt. Etna to the eruptive activity (Allard et al. 1991; D'Alessandro et al. 1997; Giammanco et al. 2007; Camarda et al. 2012; De Gregorio et al. 2014). In contrast, less attention has been given to the heat released by the steaming areas present at various altitudes and around the rim of the summit craters. It could be due to anomalies of the soil temperature—resulting in weak heat fluxes—being difficult to distinguish from the normal background when only discontinuous sampling is performed (e.g., Bonneville et al. 1985; Bonneville and Gouze 1992; Madonia et al. 2013; Maucourant et al. 2014). The thermal surface has though been measured using satellite data firstly by Bonneville et al. (1985) and by Bonneville and Kerr (1987) who also compared the thermal images with shallow ground temperatures (depth 0.03 m). Moreover, the association of thermal areas with anomalous degassing of CO_2 suggests a common hydrothermal source (e.g., Macourant et al. 2014). The isotopic signature and chemical composition of emitted fluids can reveal the character of such a hydrothermal source that is the relative contribution of magmatic, meteoric, and/or marine fluids (e.g., Aizawa et al. 2016; Liotta et al. 2010). The delays between geochemical signals and volcanic events can reveal underground connections within, and between, the plumbing and hydrothermal system (i.e., Alparone et al. 2004; Pecoraino and Giammanco 2005; Behncke et al. 2014; Giammanco et al. 2016).

With the aim of detecting a connection between an active fracture system and ongoing volcanic activity, we investigated a steam-heated soil (SHS) on the upper northeast flank of Mt. Etna close to fractures and eruptive fissures belonging to the northeast rift zone (NE rift, Fig. 1) (Neri et al. 2011, 2016). This SHS is located close to the eruptive fissure (BTL fumaroles in Figs. 2 and 3) that opened in 2002 at about 2500 m a.s.l. We set up a new monitoring site (BTL station in Figs. 2 and 3), and here we present the recorded variations in soil temperature and the application of the SHS monitoring method. Data (amounting to nearly 26,000 data points) were acquired hourly from September 2009 to September 2012 along a vertical soil profile (down to a depth of 60 cm) in the direction of the main component of the surface heat flow. The heat flux anomalies from the ground have been evaluated over a 3-year period. This allows changes in the hydrothermal release to be related to levels of volcanic activity to be assessed, discussed, and compared with published geophysical data. Figure 3 gives a sketch of a 3D section of the system tracked, where dikes depart from the central conduits. The sketch suggests a connection between

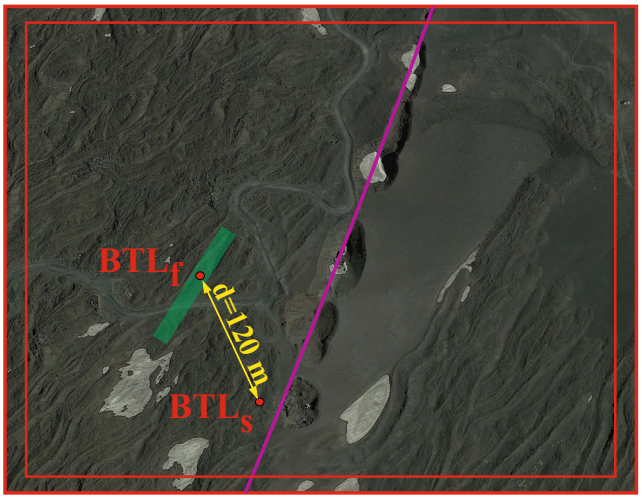

Fig. 2 Satellite image (Google Earth) of the monitoring site BTL_s and fumarole (BTL_f) sampled by Pecoraino and Giammanco (2005) and Liotta et al. (2010). The thick green line indicates a zone of low-temperature fumaroles

the surface thermal activity around the fumaroles along the active NE rift and the eruptive vents on the southeast flank.

Surface steam loss around Mt Etna

Steam is emitted from many areas on the slopes of Mt. Etna, some of which have been studied geochemically in terms of temperature and the chemical and isotopic compositions of CO_2 (Giammanco et al. 1998; Pecoraino and Giammanco 2005). However, the locations of many of the steaming zones are still unknown. Individual steaming areas can appear or disappear after every eruption on the upper slope as well as at the top of the craters (e.g., Bonneville et al. 1985; Bonneville and Kerr 1987). New steaming zones are caused by the active tectonic strain allowing hot fluid to escape through the permeable framework of fractured rocks and pyroclastic layers.

The most evident steaming areas at Mt. Etna that have already been investigated geochemically or by combined approaches are as follows:

a) An area located on the south rift near TDF in Fig. 1 (Pecoraino and Giammanco 2005; Giammanco et al. 1998) at an average altitude of 2900 m a.s.l. The south rift consists of a group of parallel fissures running in a north-south direction, starting from the summit crater on the southeastern flank of Mt. Etna. The heat released in 1988 was evaluated for the first time by Aubert (1999) using the SHS method. Tests were subsequently performed in 2009 and 2012 (Diliberto, unpublished data), and the recorded temperature profiles suggested that this location was not suitable for continuous monitoring using the SHS method proposed by Aubert (1999) due to the presence of a liquid phase. Coarse and fresh scoria has been frequently added to the soil profile by recent explosive activity from the summit craters. The inhomogeneity of the shallow permeability due to the presence of coarse and fresh scoria in this area

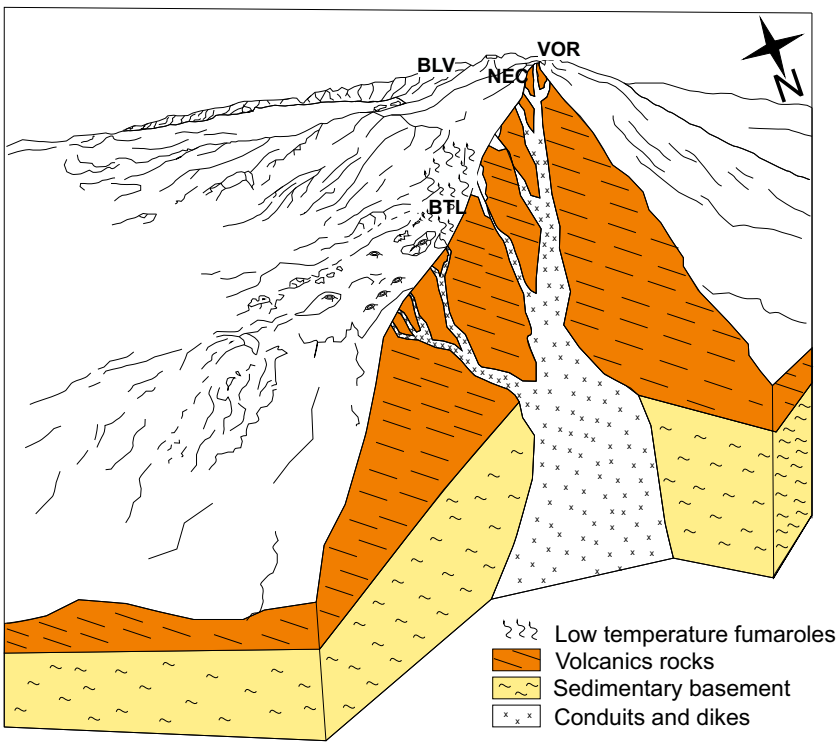

Fig. 3 Schematic model of the plumbing system with volcanic features. Refer to caption of Figs. 1 and 2 for the acronyms

allows the steam to expand and condense very close to the ground surface. Other authors have also chosen this area as a test site for obtaining information on the potential reactivation of the summit craters (Maucourant et al. 2014).

b) The Belvedere steaming area (BLV in Fig. 1), which is located on the rim of Valle del Bove on the south rift at an altitude of about 2720 m a.s.l., is characterized by significant CO_2 fluxes (Pecoraino and Giammanco 2005; Di Martino et al. 2013; De Gregorio et al. 2014).

c) The rim of the Voragine crater at 3260 m a.s.l. (VOR in Fig 1). In this area, Harris et al. (1997) already observed a highly radiating surface, north of the active lava field, while they were retrieving surface temperatures by satellite data from very high resolution radiometer (AVHRR), during the March to July 1985 eruption. That thermal anomaly corresponded to the cooling surface from a previous activity, dated April to October 1984 (Harris et al. 1997). Later on, in the same area, the SHS thermal monitoring revealed advective degassing (Madonia et al. 2013), still active and correlated to the 2008–2009 subterminal eruption from the SEC crater (Bonaccorso et al. 2011a,b). However, the location of this unstable area of the volcanic cone makes it extremely dangerous to either monitor changes in the heat flow by direct measurements or set up a long-term program of geochemical investigations.

d) An area named "hornitos" located at 3000 m a.s.l., southeast of Voragine (VOR in Fig. 1), which has been covered by lava and tephra erupted by the southeast crater (SEC in Fig. 1). This area lies on the south rift in the proximity of the Vulcarolo fumarole field (Fig. 1) and is actively degassing (Alparone et al. 2004; Madonia et al. 2013).

e) The NE rift (Fig. 1) is a volcano-tectonic feature visible on the northeast flank of the volcano which is subject to (1) frequent magma emplacement events involving dike intrusion and eruption along the rift (Patanè et al. 2005) (2) seismic energy release resulting from magma emplacement (Patanè et al. 2003, 2006), and (3) transient slipping of the Pernicana fault system (Ruch et al., 2013). A line of craters formed during the 2002–2003 eruption (BTL in Figs. 2 and 3) and these are aligned with the NE rift, and the gas emissions from some low-temperature fumaroles in the proximity of the upper part of this crater row have been sampled and analyzed (Pecoraino and Giammanco 2005). Studies of these steam emissions suggest that the emitted fluids are connected to the main feeding system of the volcano (Pecoraino and Giammanco 2005; Liotta et al. 2010). Samples collected by us at the BTL fumaroles (BTL_f in Fig. 2) in 2009, before the eruptive period discussed in this paper, showed a gas mixture of CO_2 (predominating) and CH_4 with high degrees of air contamination.

Notwithstanding the different locations, both the south rift and NE rift are fed by dikes extending from the main magma conduit (Fig. 3), rather than being connected to different, individual shallow magmatic chambers individually (Giammanco et al. 2016 and references therein).

With the aim of detecting a potential connection between an active fracture system and the ongoing volcanic activity, we set up a monitoring site on the NE rift at an altitude of 2480 m a.s.l., i.e., in a summit-proximal location (BTL station in Fig. 2). It is worth noting that this site was not affected by surface changes during the period of acquisition, since it is on the flank opposite the main direction of the pyroclastic fall, that tend to be in the direction of the prevailing wind (E to SE), and lava flows erupted by the new southeast crater (New Southeast Cone in Fig. 4). Any physical changes in coverage are thus simply due to seasonal variations in snow cover and melt.

Monitoring method

Tabbagh and Trezeguet (1987) introduced the theoretical background for evaluating and monitoring thermal releases, showing a first set of field measurements made in the summit area of Mt. Etna (TDF in Fig. 1) during 1982. Afterwards Aubert (1999) applied the same monitoring method through a field deployment of seven buried thermocouples separated by 0.1 m of soil, down to a depth of 1.2 m in 1998. The measurements by Aubert (1999) on the southern flank of Mt. Etna (TDF in Fig. 1) showed heat flux values ranging from 10 to 300 $W \times m^{-2}$. The SHS method has been applied continuously under other very different conditions: at New Hebrides (Tabbagh and Lardy 1993; Lardy and Tabbagh 1999), on Mt. Etna during eruptive activity (Madonia et al. 2013), and on Vulcano Island in a close conduit volcanic system away from the main fumarole field (Diliberto 2017; Cannata et al. 2012; Aubert et al. 2008).

The best site for monitoring heat flux using the SHS method is where the condensation zone occurs just beneath the monitored profile. Within the upper layer (from Z1 up to the ground level in Fig. 5a, b), whenever the ascending steam is completely condensed, the convective component of the heat transport becomes negligible, as does any process implying heat production or consumption. Below the Z1 depth, the soil temperature is enhanced by the steam condensation which dominates over temperature conductive exchanges between the ascending fluids and the soil. Figure 5a shows a sketch of the soil profile, and Fig. 5b shows a model of the temperature gradient present in the monitored soil. The layer between depth Z1 and the surface (CdHT in Fig. 5a) is generally dry and is dominated by the conductive transfer law (Fourier's Law), and so $\delta T/\delta Z$ is linear (Fig. 5b). The heat flux is essentially convective below level Z2 (CvHT in Fig. 5a) and the temperature of the steam is buffered by the boiling point, which is about 91 °C at this altitude, corresponding to the temperature measured at the nearby fumaroles (Fig. 2). A

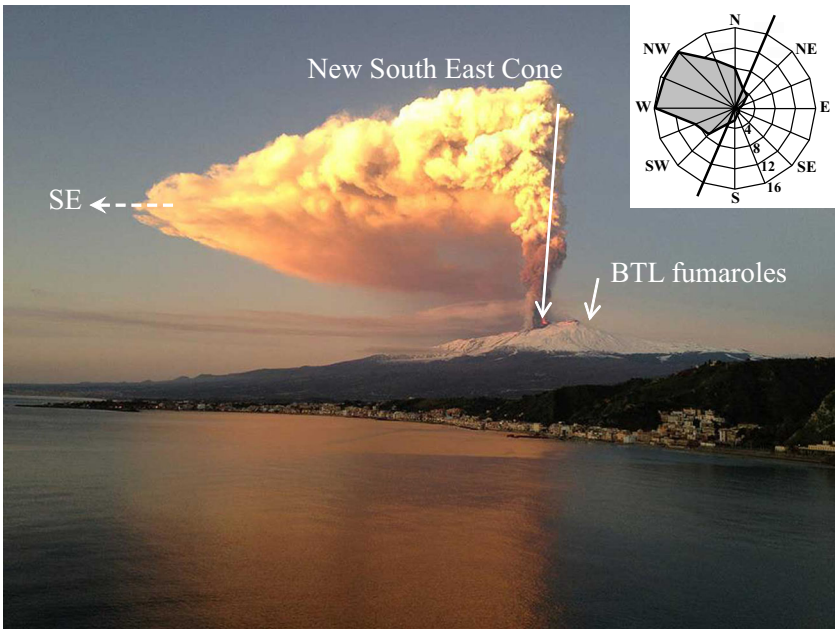

Fig. 4 View of Mt. Etna showing plume dispersion from the erupting crater (5 January 2012) and the monitored site (4 km to the N). In the top-right corner, the rose diagram indicates the main wind direction. Photo credit (http://www.youreporter.it/foto Eruzione_5_gennaio_2012)

liquid phase dominates in the layer between Z2 and Z1 due to the condensation of hydrothermal steam, so that the heat transfer here is partially conductive (CdHT in Fig. 5a) and partially convective (CvHT in Fig. 5a). The success of this monitoring approach is thus crucially dependent on the site location and physical conditions of the ground. Two conditions need to hold when estimating the heat flux from the temperature gradient: (1) the site must be far from the boiling temperature and (2) the heat flux should be unidirectional along the monitored profile (the Z direction and depth over Z1 in Fig. 5b) and conductive at the top.

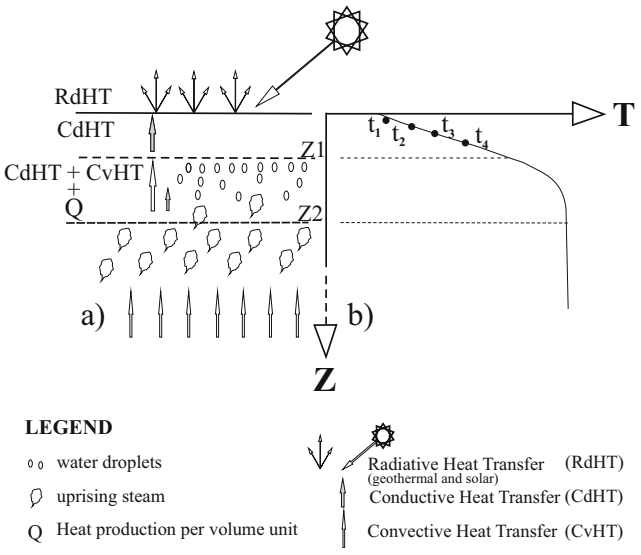

Fig. 5 **a** System model of the monitored soil profile with the main heat transfer processes. **b** Hypothetical temperature gradient at BTL station: conductive transfer dominates, and δT/δZ is linear between Z1 and the surface (redrawn from Diliberto 2017)

Figure 6 shows the temperature distribution along the monitored profile at three different times. Each set of data shows a high linear correlation calculated among the values recorded at the four monitored depths at the same time (*R* in Fig. 6). The linear temperature gradient has been extrapolated to the boiling temperature to evaluate the lowest limit of the conductive layer. The limit of the conductive layer is deeper than the last extrapolated values shown in Fig. 6. Above these limits (i.e., above the Z1 depths Figs. 5 and 7), the simplified heat flow equation (ϕ_H) can be applied up to the ground level (Aubert 1999; Tabbagh and Trezeguet 1987):

$$\phi_H = \lambda(t_4 - t_2)/(z_{t4} - z_{t2}) \quad (1)$$

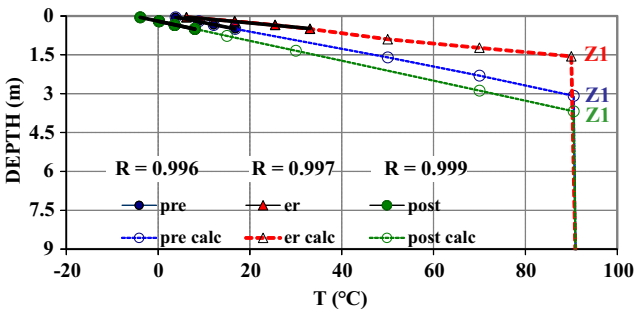

Fig. 6 Examples of the temperature distribution along the monitored profile during the three different eruptive phases. The profiles refer to three phases of volcanic activity at Mt. Etna: October 3, 2009 for the pre-eruptive period (pre), October 6, 2011 for the eruptive period (er), and April 10, 2012 for the post-eruptive period (post). The respective correlation coefficients (*R*) for the profiles are shown. The Z1 depths are extrapolated by the best fit equations

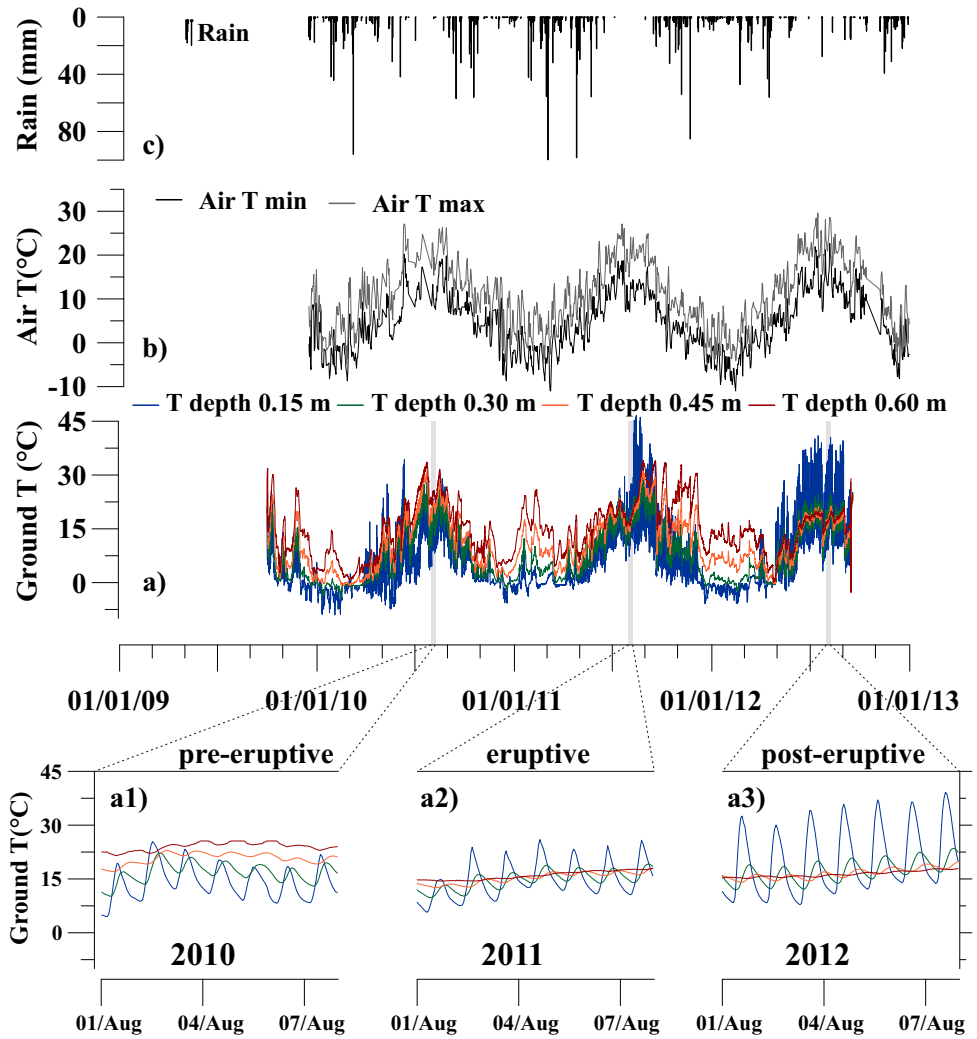

Fig. 7 **a** Time variations of temperature at four depths (in meters) within the shallow layer governed by conductive heat transfer (linear correlation, $R > 0.990$; a1, a2, a3). Detail of the ground temperatures recorded during the first week of August in 2010, 2011, and 2012 as an example of the pre-eruptive, eruptive, and post-eruptive periods, respectively. **b** Time variations of air temperature recorded at the WS-EN meteorological station. **c** Rainfall recorded at the WS-EN meteorological station

where t_4 and t_2 are the temperatures (in kelvin) measured at the different levels in the ground, z_{t4} and z_{t2} are the corresponding reference depths (in meters), and λ is the thermal diffusivity of the ground.

In the following calculation, the uppermost monitored level (t_1 located at depth of 0.15 m below the ground surface) was excluded to avoid the external influence of the daily variation due to solar heating. Moreover, λ was assumed to be constant, at $\lambda = 0.8$ W m^{-1} K^{-1} (Aubert 1999; Tabbaugh and Trezeguet 1987). This assumption applies only to dry ground conditions (i.e., in the absence of water and steam), which fulfills the necessary conditions highlighted by the linear correlation of temperatures ($R > 0.990$) among the four monitored levels. Sixty-six percent of the temperature data fulfilled this condition and have been considered in further processing.

The monitoring site was located in the proximity of a line of fumaroles (indicated as BTL_f in Fig. 2) along the NE rift, at 2470 m a.s.l. The BTL_s (Fig. 2) monitoring station is about 120 m NW direction from the low-temperature fumaroles on top of the 2002–2003 eruptive fissure. The shallow temperature appeared homogeneous around the selected point at the time of the survey. At the same time, and prior to the excavation, the temperatures measured along a vertical profile indicated a positive heat flux toward the surface, even at the time of maximum solar radiation (11:00 a.m. during summertime), with temperatures of 20 and 32 °C at depths of 0.15 and 0.60 m, respectively (the shallowest and deepest positions measured). These temperature measurements were made in the undisturbed soil and could be accounted for by an effective bottom-sourced (hydrothermal and/or magmatic) heat flux and fulfilled both of the

required conditions for heat flux monitoring. The temperature increased with depth, which is opposite to the normal condition expected at the time of the first survey (noon on a clear-sky day in summer). A vertical line with four PT1000 sensors (range − 40 to 150 °C, accuracy ± 0.2 °C, resolution ± 0.1 °C) was connected to an EBRO EBI 2T-313 four-channel data logger which was then buried at a depth of 0.60 m within the loose volcanic breccia. The temperature variations within this undisturbed ground profile have been recorded hourly for about 3 years at depths of 0.15, 0.30, 0.45, and 0.60 m.

Results

Temperature data

The recorded temperatures varied markedly throughout the analyzed period (Fig. 7a). The position chosen at the starting time appeared to be a ground with surface temperature influenced mainly by solar radiation, and the temperature range along the monitored vertical axis was far below the boiling temperature. Overall, the BTL_s site can be considered to be only weakly heated by steam, based on comparisons with temperature profiles recorded elsewhere. At the shallowest monitored level (0.15-m deep; Fig. 7a), the temperature ranged from − 9 to 46 °C, while it ranged over a narrower range (0–34 °C) at a depth of 0.60 m. The recorded temperatures peaked at all monitored levels during summer 2011 (Fig. 7a). Higher temperatures were generally measured at the deepest level, except in August 2011 and after April 2012. Moreover, during these two periods, a very high daily fluctuation was only recorded at a depth of 0.15 m (Fig. 7a).

Our time series can be compared with the local meteorological parameters by considering the records from two weather stations located at two ski resorts on Mt. Etna: (1) weather station Etna south, located at UTM 499936 E and 4172571 N, and 1935 m a.s.l. and (2) weather station Etna north (WS-EN in Fig. 1), located at UTM 503250 E and 4182972 N and 1825 m a.s.l. Data from these two weather stations do not indicate large differences in the time variations of temperature and rainfall during the analyzed 3-year period. The BTL and WS-EN sites are on the same flank and have no physical barriers between them, and so we assumed that atmospheric variations would affect the two sites in the same way. The air temperature at BTL should be about 4.2 °C lower than that recorded at WS-EN (Fig. 7b), based on the average adiabatic thermal gradient 6.5 °C km^{-1} (e.g., Tomasi et al., 1997).

A visual comparison of air and soil temperatures (Fig. 7a, b) reveals the presence of a direct relationship between them, such as in common cyclic behavior due to seasonal and daily solar radiation effects. However, panels a1, a2, and a3 in Fig. 7 show that under the same weather conditions (i.e., maximum solar radiation and lowest rainfall), different years show very different temperature fluctuations in the ground. As we expected, the atmospheric conditions affected the shallowest monitored level (i.e., t_1 at 0.15 m depth) more than lower levels. The external perturbations, due to occasional combinations of certain physical features (e.g., rainfall, wind, and melting ice), exert unpredictable effects, mostly on the short-term variations and during the winter season (Fig. 7c). However, the temperature distribution in the ground appears related not only on the atmospheric agents but also to other causes. These data could thus reveal a relationship with changes of the bottom-sourced heat flux that in turn depend on the local dynamics of volcanic activity.

Limit of the conductive layer

In accordance with the models in Fig. 5 and the examples shown in Fig. 6, the linear extrapolation of the temperature distribution along the monitored profile has been used to trace the depth variations of steam ascending beneath BTL. The Z1 depths are the uppermost limits suggested by the $\delta T/\delta Z$ slopes for the boiling conditions at TBL site (91 °C; 0.74 atm). As a result, Z1 can be considered as the reference depths for the upper limit of a convective front (CvHT; Z2 in Fig. 5). To obtain the Z1 depths shown in Fig. 8, we first filtered out the presence of water in the layer, by excluding the temperature profiles having linear correlation coefficients $R \leq 0.990$. Then, we extracted the data recorded at nighttime (hour 0.00) from the residual subset of data (17,160 profiles), so as to filter out the daily modulation caused by the diurnal cycle of solar radiation. Finally, the linear extrapolation was calculated on the temperature records from the second, third, and fourth levels only, to further reduce the thermal effects of atmospheric factors affecting essentially the shallowest level.

Table 1 shows the descriptive statistics of the Z1 depths extrapolated during different phases of volcanic activity, and Fig. 8 shows the relative temporal variations. The volcanic phases have been assigned using the volcano observation network (Behncke et al., 2014; INGV-Ct). At the monitored site (BTL in Figs. 2 and 3), the limit of the conductive layer varied within the range from 1.5 to about 30 m of depth below the ground level (Depth bgl, Fig. 8). During the first eruptive period, that is from January 2011 until September 2011, the range and the variance of Z1 depths have not changed much in respect to estimations concerning the pre-eruptive period (Table 1). However the relative time variations of Z1 depth show that the convective front had been less stable in the pre-eruptive phase. Especially from October 2009 to June 2010, Z1 depths frequently had values greater than 6 m (Fig. 8). While the conductive layer has remained confined within 4 m of the surface during the eruptive periods, such as from January to March 2011 and from October 2011 to March 2012 (Fig. 8). The general deepening of the base of conductive layer since March 2012 suggested a relative contraction of the convective front, after the eruption end (Fig. 8; Table 1).

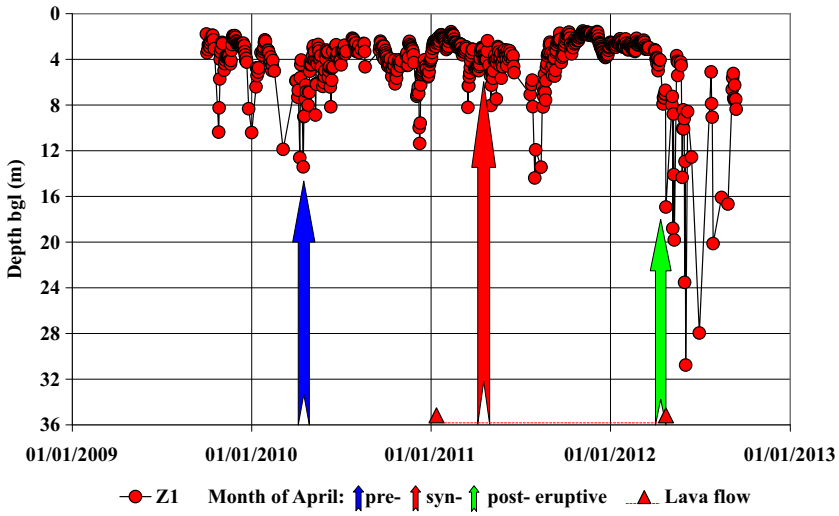

Fig. 8 Time variations of the Z1 depths extrapolated from the temperature profiles, only extrapolations with $R > 0.990$ are considered. The three colored arrows highlight the Z1 values extrapolated during the month of April in 2010 (blue), 2011 (red), and 2012 (green). In the legend "pre-" stands for the pre-eruptive period, "syn-" stands for the eruptive period, and "post-" is the post-eruptive period. The red triangles at the bottom indicate the periods of active lava flow

The profiles have thus been analyzed during three different phases of volcanic activity: pre-eruptive, eruptive, and post-eruptive (Fig. 8). The Z1 depth limits were shallowest during an eruption and deepest after an eruption. The shallowest Z1 depths were found during the eruptive period, indicating ascent of the condensation level and an increase in heat flux from the diffusive layer directly related to magma ascent. In contrast, during the pre-eruptive and post-eruptive phases, deeper levels of condensation and lower heat fluxes were registered. Even if the end of the linear trend and the relative Z2 depths are not properly constrained, it is clear from Fig. 8 that the $\delta T/\delta Z$ slope increased during the productive period of the eruption, being associated with an increase in the heat flux. The temperature trends recorded from September 30, 2009 to September 14, 2012 at four levels along a vertical profile frequently showed linear correlations (i.e., R close to 1) adding confidence to our temporal trends and interpretations.

Heat flux from the soil

The heat flux from the soil was calculated at the BTL station by applying the simplified heat flow equation (Eq. 1) to the same subset of data described in the previous section. Three different ranges of heat flux from the soil can be distinguished in Fig. 9, during the pre-eruptive, eruptive, and post-eruptive phases. Figure 10 compares the 30 day-period moving averages of the SHS heat flux with the cumulative eruption rates of lava and pyroclasts (Behncke et al. 2014) and with the monthly average air temperatures. Differences among the range of heat fluxes from the steaming ground (white arrows 1–4 in Fig. 10) are still evident in the smoothed curve. Moreover, the higher rate of erupted material is associated with the main increase in the SHS heat flux (arrow 3 in Fig. 10) that began on July 1, 2011, reaching the highest recorded value in November 2011. In contrast, there is a clear inverse correlation between SHS flux and air temperature during the summit activity in 2011 and 2012, although such a correlation was less evident during the pre-eruptive period in 2009 and 2010.

Three different phases of volcanic activity (pre-eruptive, eruptive, and post-eruptive) are also identified in Fig. 10 from the cumulative volume of erupted material. The range of heat fluxes peaked during the eruptive period, from January 2011 until April 2012 (red arrow in Fig. 9 and arrows 2 and 3 in Fig. 10). An intermediate range characterized the pre-eruptive period (blue arrow in Fig. 9 and arrow 1 in Fig. 10) from September 2009 to December 2010. During the post-eruptive activity, a narrower range and the lowest heat flux

Table 1 Descriptive statistics for the Z1 depths extrapolated during the three eruptive phases

Volcanic phase	Start	End	Variance (m^2)	Average (m)	Min (m)	Max (m)	Number of profiles having $R > 0.990$
Pre-eruptive	01/10/09	11/01/11	3.3	4.2	1.8	13.4	296
Eruptive	12/01/11	24/04/12	3.0	3.7	1.9	16.9	381
Post-eruptive	24/04/12	13/09/12	43.6	10.8	3.7	30.8	38

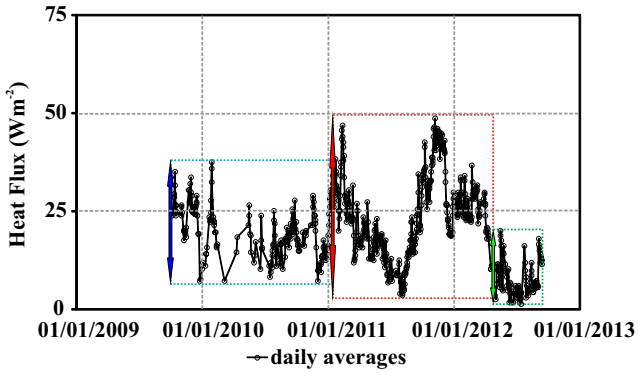

Fig. 9 Heat flux variations in SHS retrieved from our thermocouple data. The blue, red, and green arrows and dashed boxes indicate the ranges of heat flux (daily averages) for the pre-eruptive, eruptive, and post-eruptive phases. Only extrapolations with data validated by $R > 0.990$ are considered

were observed (green arrow in Fig. 9 and arrow 4 in Fig. 10). At this point, the SHS had probably reached the local background range. In this last period, the modulation of heat flux from the ground was dominated by external factors.

Discussion

A geochemical approach based on long-term monitoring makes it possible to follow the changes in energy released from hydrothermal and/or magmatic sources in real time (e.g., Inguaggiato et al. 2018; Paonita et al. 2013; Chiodini et al. 2005; Matsushima et al. 2003; D'Alessandro et al. 1997; Bonfanti et al. 1996a,b). However, systematic observational timescales and a wide multidisciplinary approach are necessary to interpret the observed temporal variations

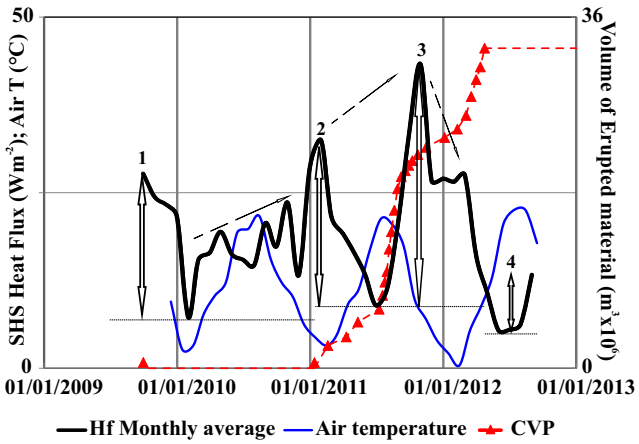

Fig. 10 Heat flux (Hf) variations in SHS and cumulative volume of erupted material (CVP, values on the right axis, Behncke et al. 2014; Bonaccorso and Calvari 2013). The white arrows indicate the ranges represented by the mean term variations. The dashed arrows give the SHS trends. The thin lines indicate the minimum values of heat flux observed during the different phases

in volcanic heat flux (e.g., Harris 2013 and references therein; Stix and Gaonach 2000). With this in mind, coupled with the low intensity of the thermal anomaly involved, we monitored soil temperature changes at a specific site in order to identify variations in the bottom-sourced heat flux. Our results are the first application of the method proposed by Tabbaugh and Trezeguet (1987) and Aubert (1999) during a complete volcanic cycle. During the studied period starting from January 2011, the eruptive activity of Mt. Etna generated the New Southeast Crater on the flank of the SEC (Behncke et al. 2014). This eruption was characterized by high eruption rates of lava and Strombolian activity until April 24, 2012, which was followed by a period of collapse (Behncke et al. 2014). The BTL monitoring site (Figs. 2 and 3) is in proximity to an eruptive fissure (which last erupted during 2002–2003), about 4 km from the vents that erupted during the monitored period (SEC, Fig. 1). Although the depth limit of the convective heat transfer regime has not been fully constrained, we used the recorded data to detect variations in the depth of convective front (i.e., the depth of Z1). Such variations should reflect changes in fluid pressure in the shallow hydrothermal or magmatic system. Following the $\delta T/\delta Z$ slope changes, the upper convective front moved during the different volcanic phases (Fig. 8). In particular, the limit of the conductive layer (Z1) tended to rise before the start of a new eruption. The lowest variance in the conductive layer has been observed between mid-August 2011 and March 2012, while the volcano was in continuous eruption. The deepest positions of the conductive layer were observed after the end of the eruptive period (Fig. 8), and this result can be interpreted as a contraction of the convective system feeding the fumaroles of the NE rift. On the NE rift, the shallow hydrothermal circuit, which apparently was not involved in the eruption, thus showed fluctuations of the convective front related to the eruptive activity, resulting from heat flux variations of the soil. The increases of the intensity of the thermal anomaly around low-temperature fumaroles reflected, at the same time, the ascent of the condensation level driven by the increased pressure of hydrothermal fluids during periods of activity.

We thus find a direct relationship between the low-temperature fumaroles and the eruptive activity. We infer that the increase of fluid pressure in the magmatic source feeding the impending eruption provoked an increase in steam release along the Northeast Rift and consequently enhanced SHS heat flux. The energy discharge of magmatic origin, which was associated with eruption at the southeast crater, then resulted in high and steady levels of thermal release along the NE rift. Variations in fluid pressure associated with volcanic activity thus result in thermal effects over a wide area. Tracing its changes by remote monitoring is thus a valid tool for assessing the activity levels of the system in an eruptive and pre-eruptive phase.

Conclusion

We applied an empirical approach to compare different time series of data in order to identify variations related to the energy released by an active geothermal, hydrothermal, and magmatic system. The continuous monitoring system was based on the temperature monitoring method applied to soil heat fluxes by Tabbagh and Lardy (1993), Lardy and Tabbagh (1999), Aubert (1999), Aubert et al. (2008), and Diliberto (2017). Our temperature monitoring station yielded reliable time series of conductive heat transfer in which we could identify different ranges related to the different stages of activity: pre-eruptive, eruptive, and post-eruptive.

Low-temperature fumaroles are buffered at the boiling point. This buffering of temperature makes the temperature of fumaroles unsuitable for monitoring, because only strong decreases in temperature can be detected. The present method, applied to the SHS around fumaroles, yielded a method capable of overcoming the limit imposed by the buffering condition. In SHS method, the steam condensation occurs below the ground level, where it enhances local heat release, this being an exothermic process (e.g., Chiodini et al. 2005). Here, the temporal resolution of continuous monitoring makes it possible to track and define any change in steam release.

A new eruptive cycle began during our monitoring period. Over a time interval of 1082 days (September 2009–September 2012), all changes in the soil heat flux were linked to variations in activity, distinguishing between pre-eruptive, eruptive, and post-eruptive regimes. Our monitoring method thus allowed us to identify a connection between monitored steaming zone on the NE rift of Etna and the eruptive conduits that fed the most recent volcanic cycle at the SE crater.

Such a simple monitoring method gives a measure of the secondary thermal effects exerted by magma dynamic. Tracking variation in these effects offers great monitoring potential. For example, an increase in SHS heat flux could suggest that the intensity of an eruption is going to increase and a decrease could herald cessation. If the monitoring station is located on a fractures network connected to the eruptive conducts, this system offers a dataset that can be used as a reference for evaluating magma flux conditions when the other observational data are discontinuous.

Thermal monitoring allowed us track over the energy released from a thermal anomaly along Etna's NE rift zone between 2009 and 2012 and to relate variations in this flux to activity at the summit craters about 4-km distant. The analysis of soil temperature data allowed us to identify heat flux variations related to the continuous release of thermal energy and to compare with trends apparent in time series of observational data. We find that real-time, continuous, and operational monitoring of heat release reduces the risk of incorrect interpretations, interpolated by other discontinuous observations, allowing the heat flux response of the system to increase and diminish mass fluxes into the system to be tracked. Building on previous work from Japan (Matsushima et al. 2003; Sekioka and Yuhara 1974; Ohara and Okamoto 1980), Vulcano (Diliberto 2017; Cannata et al. 2012; Aubert et al. 2008), Vanuatu (Lardy and Tabbagh 1999), and Etna (Madonia et al. 2013; Aubert 1999; Tabbagh and Trezeguet 1987), we thus argue that the SHS heat flux method provides a new parameter to be considered for continuous, operational monitoring and for generation of deterministic models aimed at interpreting volcanic activity in terms of effects on hydrothermal fluid circulation.

Acknowledgments The National Department of Civil Protection supported the acquisition of data presented in this work. We are grateful to A. Harris, T. Nishimura, and the anonymous reviewers for comments and excellent suggestions that improved our original manuscript and helped us to underline the results.

References

Aizawa K, Sumino H, Uyeshima M, Yamaya Y, Hase H, Takahashi HA, Takahashi M, Kazahaya K, Ohno M, Arunwan TR, Ogawa Y (2016) Gas pathways and remotely triggered earthquakes beneath Mount Fuji, Japan. Geology 44(2):127–130. https://doi.org/10.1130/G37313.1

Allard P, Carbonnelle J, Dajlevic D, Le Bronec J, Morel P, Robe MC, Maurenas JM, Faivre-Pierret R, Martin D, Sabroux JC, Zettwoog P (1991) Eruptive and diffuse emissions of CO_2 from Mount Etna. Nature 351(6325):387–391. https://doi.org/10.1038/351387a0

Alparone S, Andronico D, Giammanco S, Lodato L (2004) A multidisciplinary approach to detect active pathways for magma migration and eruption at Mt. Etna (Sicily Italy) before the 2001 and 2002–2003 eruptions. J Volcanol Geotherm Res 136(1-2):121–140. https://doi.org/10.1016/j.jvolgeores.2004.05.014

Aubert M (1999) Practical evaluation of steady heat discharge from dormant active volcanoes: case study of Vulcarolo fissure Mount Etna Italy. J Volcanol Geotherm Res 92(3-4):413–429. https://doi.org/10.1016/S0377-0273(99)00088-8

Aubert M, Diliberto IS, Finizola A, Chébli Y (2008) Double origin of hydrothermal convective flux variations in the Fossa of Vulcano (Italy). Bull Volcanol 70(6):743–751. https://doi.org/10.1007/s00445-007-0165-y

Azzaro R, Branca S, Gwinner K, Coltelli M (2012) Volcano-tectonic map of Etna volcano. Ital J Geosci (Boll Soc Geol It) 131:153–170. https://doi.org/10.3301/IJG.2011.29

Barberi F, Carapezza ML, Valenza M, Villari L (1993) The control of lava flow during the 1991–1992 eruption of Mt. Etna. J Volcanol Geotherm Res 56(1-2):1–34. https://doi.org/10.1016/0377-0273(93)90048-V

Behncke B, Branca S, Corsaro RA, De Beni E, Miraglia L, Proietti C (2014) The 2011–2012 summit activity of Mount Etna: birth growth and products of the new SE crater. J Volcanol Geotherm Res 270:10–21. https://doi.org/10.1016/j.jvolgeores.2013.11.012

Byrdina S, Revil A, Pant SR, Koirala BP, Shrestha PL, Tiwari DR, Gautam UP, Shrestha K, Sapkota SN, Contraires S, Perrier F (2009) Dipolar self-potential anomaly associated with carbon dioxide and radon flux at Syabru-Bensi hot springs in central Nepal. J Geophys Res 114(B10):B10101. https://doi.org/10.1029/2008JB006154

Bombrun M, Spampinato L, Harris A, Barra V, Caltabiano T (2016) On the transition from strombolian to fountaining activity: a thermal energy-based driver. Bullettin Volcanol 78(2):15. https://doi.org/10.1007/s00445-016-1009-4

Bonaccorso A, Calvari S, Garf G, Lodato L, Patane D (2003) Dynamics of the December 2002 flank failure and tsunami at Stromboli

volcano inferred by volcanological and geophysical observations. Geophys Res Lett 30(18):1941. https://doi.org/10.1029/2003GL017702

Bonaccorso A, Bonforte A, Calvari S, Del Negro C, Di Grazia G, Ganci G, Neri M, Vicari A, Boschi E (2011a) The initial phases of the 2008–2009 Mount Etna eruption: a multidisciplinary approach for hazard assessment. J Geophys Res 116(B3):B03203. https://doi.org/10.1029/2010JB007906

Bonaccorso A, Cannata A, Corsaro RA, Di Grazia G, Gambino S, Greco F, Miraglia L, Pistorio A (2011b) Multidisciplinary investigation on a lava fountain preceding a flank eruption: the 10 May 2008 Etna case. Geochem Geophys Geosystem 12(7):Q07009. https://doi.org/10.1029/2010GC003480

Bonaccorso A, Calvari S (2013) Major effusive eruptions and recent lava fountains: balance between expected and erupted magma volumes at Etna volcano. Geophys Res Lett 40(23):6069–6073. https://doi.org/10.1002/2013GL058291

Bonfanti P, D'Alessandro W, Dongarrà G, Parello F, Valenza M (1996a) Medium term anomalies in groundwater temperatures before 1991–93 Mt Etna eruption. J Volcanol Geotherm Res 73(3-4):303–308. https://doi.org/10.1016/0377-0273(96)00026-1

Bonfanti P, D'Alessandro W, Dongarrà G, Parello F, Valenza M (1996b) Mt Etna eruption 1991–1993: geochemical anomalies in groundwaters. Acta Vulcanol 8(1):107–109

Bonneville A, Vasseur G, Kerr Y (1985) Satellite thermal infrared observations of Mt. Etna after the 17th March 1981 eruption. J Volcanol Geotherm Res 24(3-4):293–313. https://doi.org/10.1016/0377-0273(85)90074-5

Bonneville A, Kerr Y (1987) A thermal forerunner of the 28th March 1983 Mt. Etna eruption from satellite thermal infrared data. J Geodyn 7(1-2):1–31. https://doi.org/10.1016/0264-3707(87)90061-5

Bonneville A, Gouze P (1992) Thermal survey of Mount Etna from space. Geophys Res Lett 19(7):725–728. https://doi.org/10.1029/92GL00580

Calvari S, Salerno GG, Spampinato L, Gouhier M, La Spina A, Pecora E, Harris AJL, Labazuy P, Biale E, Boschi E (2011) An unloading foam model to constrain Etna's 11–13 January 2011 lava fountaining episode. J Geophys Res 116(B11):B11207. https://doi.org/10.1029/2011JB008407

Camarda M, De Gregorio S, Gurrieri S (2012) Magma-ascent processes during 2005–2009 at Mt Etna inferred by soil CO_2 emissions in peripheral areas of the volcano. Chem Geol 330-331:218–227. https://doi.org/10.1016/j.chemgeo.2012.08.024

Cannata A, Diliberto IS, Alparone S, Gambino S, Gresta S, Liotta M, Madonia P, Milluzzo V, Aliotta M, Montalto P, (2012) Multiparametric approach in investigating hydrothermal systems: the case of study of Vulcano (Aeolian islands Italy). Pure and Applied Geophysics 169:167–182 https://doi.org/10.1007/s00024-011-0297-z

Cannata A, Spedalieri G, Behncke B, Cannavò F, Di Grazia G, Gambino S, Gresta S, Gurrieri S, Liuzzo M, Palano M (2015) Pressurization and depressurization phases inside the plumbing system of Mount Etna volcano: evidence from a multiparametric approach. J Geophys Res Solid Earth 120(9):5965–5982. https://doi.org/10.1002/2015JB012227

Chiodini G, Cioni R, Marini L, Panichi C (1995) Origin of the fumarolic fluids of Vulcano Island, Italy and implications for volcanic surveillance. Bull Volcanol 57(2):99–110. https://doi.org/10.1007/BF00301400

Chiodini G, Granieri D, Avino R, Caliro S, Costa A, Werner C (2005) Carbon dioxide diffuse degassing and estimation of heat release from volcanic and hydrothermal systems. J Geophys Res 110(B8):B08204. https://doi.org/10.1029/2004JB003542

Corsaro RA, Andronico D, Behncke B, Branca S, Caltabiano T, Ciancitto F, Cristaldi A, DeBeni E, La Spina A, Lodato L, Miraglia L, Neri M, Salerno G, Scollo S, Spata G (2017) Monitoring the December 2015 summit eruptions of Mt Etna (Italy): Implications on eruptive dynamics. Journal of Volcanology and Geothermal Research 341:53–69. https://doi.org/10.1016/jjvolgeores201704018

D'Alessandro W, Giammanco S, Parello F, Valenza M (1997) CO_2 output and $\delta 13C_{(CO2)}$ from Mount Etna as indicators of degassing of shallow asthenosphere. Bullettin Volcanol 58(6):455–458. https://doi.org/10.1007/s004450050154

De Gregorio S, Camarda M, Gurrieri S, Favara R (2014) Change in magma supply dynamics identified in observations of soil CO_2 emissions in the summit area of Mt Etna. Bullettin Volcanol 76(8):846. https://doi.org/10.1007/s00445-014-0846-2

Di Martino RMR, Camarda M, Gurrieri S, Valenza M (2013) Continuous monitoring of hydrogen and carbon dioxide at Mt Etna. Chem Geol 357:41–51. https://doi.org/10.1016/j.chemgeo.2013.08.023

Diliberto IS (2017) Long-term monitoring on a closed-conduit volcano: a 25-year long time-series of temperatures recorded at La Fossa cone (Vulcano Island). J Volcanol Geotherm Res 346:151–160. https://doi.org/10.1016/j.jvolgeores.2017.03.005

Facca C, Tonani F (1967) The self-sealing geothermal field. Bull Volcan 30(1):271–273. https://doi.org/10.1007/BF02597674

Federico C, Capasso G, Paonita A, Favara R (2010) Effects of steam-heating processes on a stratified volcanic aquifer: stable isotopes and dissolved gases in thermal waters of Vulcano Island (Aeolian archipelago). J Volcanol Geotherm Res 192(3):178–190. https://doi.org/10.1016/j.jvolgeores.2010.02.020

Federico C, Inguaggiato S, Chacón Z, Londoño JM, Gil E, Alzate D (2017) Vapour discharges on Nevado del Ruiz during the recent activity: clues on the composition of the deep hydrothermal system and its effects on thermal springs. J Volcanol Geotherm Res 346:40–53. https://doi.org/10.1016/j.jvolgeores.2017.04.007

Giammanco S, Inguaggiato S, Valenza M (1998) Soil and fumarole gases of Mount Etna: geochemistry and relations with volcanic activity. J Volcanol Geotherm Res 81(1-3):297–310. https://doi.org/10.1016/j.jvolgeores.2010.04.006

Giammanco S, Sims KWW, Neri M (2007) Measurements of ^{220}Rn and ^{222}Rn and CO_2 emissions in soil and fumarole gases on Mt Etna volcano (Italy): implications for gas transport and shallow ground fracture. Geochem Geophys Geosyst 8(10):Q10001. https://doi.org/10.1029/2007GC001644

Giammanco S, Melián G, Neri M, Hernández PA, Sortino F, Barrancos J, López M, Pecoraino G, Perez NM (2016) Active tectonic features and structural dynamics of the summit area of Mt Etna (Italy) revealed by soil CO_2 and soil temperature surveying. J Volcanol Geotherm Res 311:79–98. https://doi.org/10.1016/j.jvolgeores.2016.01.004

Harris AJL, Butterworth AL, Carlton RW, Downey I, Miller P, Navarro P, Rothery DA (1997) Low-cost volcano surveillance from space: case studies from Etna, Krafla, Cerro Negro, Fogo, Lascar and Erebus. Bull Volcanol 59(1):49–64. https://doi.org/10.1007/s004450050174

Harris AJL (2013) Thermal remote sensing of active volcanoes: a user's manual. Cambridge University Press, Cambridge. https://doi.org/10.1017/CBO9781139029346

Heasler, H., C. Jaworowski and D. Foley (2009). Geothermal systems and monitoring hydrothermal features. Geological Monitoring. R. Young and L. Norby. Boulder, Colorado, Geological Society of America. https://doi.org/10.1130/2009.monitoring(05)

Inguaggiato S, Vita F, Rouwet D, Bobrowski N, Morici S, Sollami A (2011) Geochemical evidence of the renewal of volcanic activity inferred from CO_2 soil and SO_2 plume fluxes: the 2007 Stromboli eruption (Italy). In: Inguaggiato S, Shinohara H, and Fischer T (eds) Geochemistry of volcanic fluids: a special issue in honor of Yuri A. Taran Bull Volcanol 73(4):443–456. https://doi.org/10.1007/s00445-010-0442-z

Inguaggiato S, Diliberto IS, Federico C, Paonita A, Vita F (2018) Review of the evolution of geochemical monitoring, networks and methodologies applied to the volcanoes of the Aeolian Arc (Italy). Earth Sci Rev 176:241–276. https://doi.org/10.1016/j.earscirev.2017.09.006

Lardy M, Tabbagh A (1999) Measuring and interpreting heat fluxes from shallow volcanic bodies using vertical temperature profiles: a

preliminary test. Bull Volcanol 60(6):441–447. https://doi.org/10.1007/s004450050244

Liotta M, Paonita A, Caracausi A, Martelli M, Rizzo A, Favara R (2010) Hydrothermal processes governing the geochemistry of the crater fumaroles at Mount Etna volcano (Italy). Chem Geol 278:92–104. https://doi.org/10.1016/jchemgeo201009004

Lowenstern JB, Smith RB, Hill DP (2006) Monitoring super-volcanoes: geophysical and geochemical signals at Yellowstone and other large caldera systems. Phil Trans R Soc A 364(1845):2055–2072. https://doi.org/10.1098/rsta.2006.1813

Madonia P, Rizzo A, Diliberto IS, Favara R (2013) Continuous monitoring of fumarole temperatures at Mount Etna (Italy). J Volcanol Geotherm Res 257:12–20. https://doi.org/10.1016/j.jvolgeores.2013.03.001

Maldonado LFM, Inguaggiato S, Jaramillo MT, Valencia GG, Mazot A (2017) Volatiles and energy released by Puracé volcano. Bull Volcanol 79(12):84. https://doi.org/10.1007/s00445-017-1168-y

Matsushima N, Kazahaya K, Saito G, Hiroshi Shinohara H (2003) Mass and heat flux of volcanic gas discharging from the summit crater of Iwodake volcano, Satsuma-Iwojima, Japan, during 1996–1999. J Volcanol Geotherm Res 126(3–4):285–301. https://doi.org/10.1016/S0377-0273(03)00152-5

Mattia M, Bruno V, Caltabiano T, Cannata A, Cannavo F, D'Alessandro W, Di Grazia G, Federico C, Giammanco S, La Spina A, Liuzzo M, Longo M, Monaco C, Patane` D, Salerno G (2015) A comprehensive interpretative model of slow slip events on Mt Etna's eastern flank. Geochem Geophys Geosyst 16:635–658. https://doi.org/10.1002/2014GC005585

Maucourant S, Giammanco S, Greco F, Dorizon S, Del Negro C (2014) Geophysical and geochemical methods applied to investigate fissure-related hydrothermal systems on the summit area of Mt Etna volcano (Italy). J Volcanol Geotherm Res 280:111–125. https://doi.org/10.1016/jjvolgeores201405014

Mazot A, Rouwet D, Taran Y, Inguaggiato S, Varley N (2011) CO_2 and He degassing at El Chichón volcano (Chiapas, Mexico): gas flux, origin, and relationship with local and regional tectonics. Bull Volcanol 73(4):423–441. https://doi.org/10.1007/s00445-010-0443-y.

Neri M, Acocella V, Behncke B, Giammanco S, Mazzarini F, Rust D (2011) Structural analysis of the eruptive fissures at Mount Etna (Italy). Ann Geoph 54(5):464–479. https://doi.org/10.4401/ag-5332

Neri M, Ferrara E, Giammanco S, Currenti G, Cirrincione R, Patanè D, Zanon V (2016) Soil radon measurements as a potential tracer of tectonic and volcanic activity. Sci Rep 6:24581; https://doi.org/10.1038/srep24581

Ohara S, Okamoto J (1980) Heat discharge estimate in steaming ground. J Geotherm Res Soc Jpn 2(2):13–27. https://doi.org/10.1016/j.geothermics.2004.04.002

Oskarsson N (1984) Monitoring of fumarole discharge during the 1975–1982 rifting in Krafla volcanic center North Iceland. J Volcanol Geotherm Res 22(1-2):97–121. https://doi.org/10.1016/0377-0273(84)90036-2

Paonita A, Caracausi A, Iacono-Marziano G, Martelli M, Rizzo AL (2012) Geochemical evidence for mixing between fluids exsolved at different depths in the magmatic system of Mt Etna (Italy). Geochim Cosmochim Acta 84:380–394. https://doi.org/10.1016/j.gca.2012.01.028

Paonita A, Federico C, Bonfanti P, Capasso G, Inguaggiato S, Italiano F, Madonia P, Pecoraino G, Sortino F (2013) The episodic and abrupt geochemical changes at La Fossa fumaroles (Vulcano Island, Italy) and related constraints on the dynamics, structure, and compositions of the magmatic system. Geochim Cosmochim Acta 120:158–178. https://doi.org/10.1016/j.gca.2013.06.015

Paonita A, Longo M, Bellomo S, D'Alessandro W, Brusca L (2016) Dissolved inert gases (He, Ne, and N_2) as markers of groundwater flow and degassing areas at Mt Etna volcano (Italy). Chem Geol 443(2):10–21. https://doi.org/10.1016/j.chemgeo.2016.09.018

Patanè D, De Gori P, Chiarabba C, Bonaccorso A (2003) Magma ascent and the pressurization of Mount Etna's volcanic system. Science 299(5615):2061–2063. https://doi.org/10.1126/science.1080653

Patanè D, Mattia M, Aloisi M (2005) Shallow intrusive processes during 2002–2004 and current volcanic activity on Mt. Etna. Geophys Res Lett 32(6):L06302. https://doi.org/10.1029/2004GL021773

Patané G, La Delfa S, Tanguy JC (2006) Volcanism and mantle–crust evolution: the Etna case. Earth Planet Sci Lett 241(3–4):831–843. https://doi.org/10.1016/j.epsl.2005.10.039

Pecoraino G, Giammanco S (2005) Geochemical characterization and temporal changes in parietal gas emissions at Mt Etna (Italy) during the period July 2000–July 2003. TAO 16(4):805–841 https://doi.org/10.3319/TAO.2005.16.4.805(GIG)

Peiffer L, Rouwet D, Taran Y (2015) Fluid geochemistry of El Chichón volcano-hydrothermal system. In: Scolamacchia T., Macías J. (eds) active volcanoes of Chiapas (Mexico): El Chichón and Tacaná. Active volcanoes of the world. Springer, Berlin, Heidelberg. https://doi.org/10.1007/978-3-642-25890-9_4

Revil A, Finizola A, Ricci T, Delcher E, Peltier A, Barde-Cabusson S, Colonge J (2011) Hydrogeology of Stromboli volcano Aeolian Islands (Italy) from the interpretation of resistivity tomograms self-potential soil temperature and soil CO_2 concentration measurements. Geophys J Int 186(3):1078–1094. https://doi.org/10.1111/j.1365-246X.2011.05112.x

Rizzo LA, Caracausi A, Liotta M, Paonita A, Barnes JD, Corsaro RA, Martelli M (2013) Chlorine isotope composition of volcanic gases and rocks at Mount Etna (Italy) and inferences on the local mantle source. Earth Planet Sci Lett 371-372:134–142. https://doi.org/10.1016/j.epsl.2013.04.004

Ruch J, Pepe S, Casu F, Acocella V, Neri M, Solaro G, Sansosti E (2012) How do volcanic rift zones relate to flank instability? Evidence from collapsing rifts at Etna. Geophys Res Lett 39:L20311. https://doi.org/10.1029/2012GL53683

Ruch J, Pepe S, Casu F, Solaro G, Pepe A, Acocella V, Neri M, Sansosti E (2013) Seismo-tectonic behavior of the Pernicana Fault System (Mt Etna): a gauge for volcano flank instability? Geophys Res Lett: Solid Hearth 118:4398–4409. https://doi.org/10.1002/jgrb50281

Sato M, McGee KA (1982) Continuous monitoring of hydrogen on south flank of Mount St Helens. In: Lipman PW Mullineaux DR (Eds). The 1980 eruption of Mount St Helens, Washington. Geol Surv Prof Pap 1250:209–219

Sekioka M, Yuhara K (1974) Heat flux estimation in geothermal areas based on the heat balance of the ground surface. J Geophys Res 79(14):2053–2058. https://doi.org/10.1029/JB079i014p02053

Stevens NF, Murray JB, Wadge G (1997) The volume and shape of the 1991–1993 lava flow field at Mount Etna, Sicily. Bull Volcanol 58(6):449–454 https://doi.org/. https://doi.org/10.1007/s004450050153

Stix J, Gaonach H (2000) Gas, plume and thermal monitoring. In: Encyclopedia of volcanoes. Edited by H. Sigurdsson. Academic Press, pp 1141–1164

Tabbagh A, Trezeguet D (1987) Determination of sensible heat flux in volcanic areas from ground temperature measurements along vertical profiles: the case study of Mount Etna Sicily. Italy J Geophys Res 92_B5:3635–3644 https://doi.org/10.1029/JB092iB05p03635

Tabbagh A, Lardy M (1993) Analysis of shallow heat flow measurement on Matthews and Hunter volcanoes (SW Pacific). Geothermics 22(1):65–78. https://doi.org/10.1016/0375-6505(93)90021-E

Tanguy J-C, Kieffer G, Patane G (1996) Dynamics, lava volume and effusion rate during the 1991–1993 eruption of Mount Etna. J Volcanol Geotherm Res 71(2-4):259–265. https://doi.org/10.1016/0377-0273(95)00081-X

Tomasi C, Vitale V, De Santis LV (1997) Relative optical mass functions for air water vapour ozone and nitrogen dioxide in atmospheric models presenting different latitude and seasonal conditions. Meteorog Atmos Phys 65(1-2):11–30. https://doi.org/10.1007/BF01030266